THE JOURNAL OF PHYSICAL CHEMISTRY A

Article

pubs.acs.org/JPCA

Imaging Studies of Excited and Dissociative States of Hydroxymethylene Produced in the Photodissociation of the Hydroxymethyl Radical

Chirantha P. Rodrigo, Subhasish Sutradhar, and Hanna Reisler*

Department of Chemistry, University of Southern California, Los Angeles, California 90089-0482, United States

Supporting Information

ABSTRACT: Rotational, vibrational, and electronic states of formaldehyde and *cis*-hydroxymethylene products generated in the photodissociation of the hydroxymethyl radical are investigated by sliced velocity map imaging (SVMI) following excitation of the radical to its $3p_x$ and $3p_z$ Rydberg states. SVMI of H and D photofragments is essential in these studies because it allows zooming in on low-velocity regions of the images where small threshold signals can be identified. With CH_2OD precursors, formaldehyde and hydroxymethylene products are examined separately by monitoring D and H, respectively. Whereas the main dissociation channels lead to formaldehyde and *cis*-hydroxymethylene in their ground electronic states, at higher excitation energies the kinetic energy distributions (KEDs) of H and D photofragments exhibit additional small peaks, which are assigned as triplet states of formaldehyde and hydroxymethylene. Results obtained with deuterated isotopologs of CH_2OH demonstrate that the yield of the triplet state of formaldehyde decreases upon increasing deuteration, suggesting that the conical intersection seams that govern the dynamics depend on the degree of deuteration. The rotational excitation of *cis*-hydroxymethylene depends on the excited Rydberg state of CH_2OD and is lower in dissociation via the $3p_z$ state than via the lower lying $3p_x$ and 3s states. Vibrational excitation of *cis*-HCOD, which spans the entire allowed internal energy range, consists mostly of the CO-stretch and in-plane bend modes. When the internal energy of *cis*-HCOD exceeds the dissociation threshold to D + HCO, slow D and H photofragments deriving from secondary dissociation are observed. The yields of these H and D fragments are comparable, and we propose that they are generated via prior isomerization of *cis*-HCOD to HDCO.

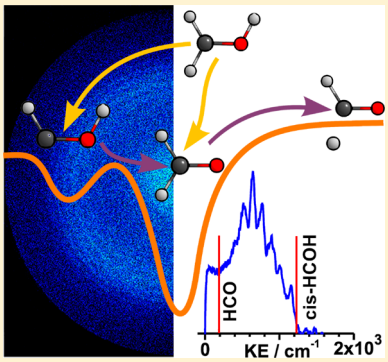

I. INTRODUCTION

Hydroxymethylene, the tautomer of formaldehyde, has been implicated in combustion and astrochemical processes, as well as an intermediate in the production of sugars, reactions of organometallic compounds, etc.[1,2] Although formaldehyde and its photoinitiated unimolecular reaction have been studied for many years,[3−5] much less is known experimentally about hydroxymethylene, the prototype hydroxycarbene. Its lowest energy *trans* isomer was isolated in the matrix and characterized using IR and UV spectroscopy,[6] and very recently, the IR spectrum was measured also in He nanodroplets.[7] The observed IR absorptions were confirmed by variational calculations of anharmonic vibrational energies.[6−8] It has also been shown that *trans*-HCOH isolated in a cold Ar matrix isomerizes via tunneling through a narrow barrier to formaldehyde with a half-life of ∼2 h, whereas HCOD is essentially stable.[6,9] The formation of hydroxymethylene as a significant product in the photodissociation of CH_2OH and its isotopologs was first reported in 2004,[10] and the production of the *trans* and *cis* isomers in the photodissociation of CH_2OH was characterized later.[11] The *trans*-HCOH isomer lies 18 264 ± 140 cm^{-1} above the zero point level of H_2CO, and the *cis*−*trans* separation is 1550 ± 40 cm^{-1}.[11] The corresponding values for HCOD are similar taking into account zero-point energy (ZPE) differences.[11]

HCOH became the focal point of theoretical attention about 30 years ago as a possible participant in the unimolecular decomposition of formaldehyde.[4,12−16] The past decade saw renewed interest in the H_2CO/HCOH system driven by new experimental results that identified a "roaming" mechanism as a significant pathway to CO + H_2 in the photodissociation of formaldehyde.[17−20] These experimental results, in turn, inspired new theoretical work, and potential energy surfaces (PESs) are now available for the S_0, S_1, and T_1 states that encompass the two tautomers, as well as the CO + H_2 and H + HCO product channels and transition states for the relevant processes.[21−24]

Especially relevant to the present study are recent calculations of the singlet−triplet gap (ΔE_{S-T}) in hydroxymethylene. Most calculated values place the gap (including ZPE) at around 25 kcal/mol (∼8740 cm^{-1}).[22,25−31] The energy difference between the T_1 states of formaldehyde and hydroxymethylene is another value that can be compared with experiments. According to Zhang et al. this energy

Special Issue: David R. Yarkony Festschrift

Received: May 24, 2014
Revised: June 30, 2014

   dx.doi.org/10.1021/jp505108k | J. Phys. Chem. A XXXX, XXX, XXX−XXX

separation (including ZPE) is 5.78 kcal/mol (2022 cm^{-1}) at the MRCISD(Q)/aug-cc-pV5Z level of theory.[22] Clearly, this energy separation is much smaller than that between the S_0 states of H_2CO and *trans*-HCOH, which has been measured at 52.2 kcal/mol (18 264 cm^{-1}).[11] The experimental value for the S_0-T_1 gap in formaldehyde is well established at 25 194 cm^{-1}.[32−35]

The geometry of ground-state HCOH (*cis* and *trans*) is planar.[6,8,29] In contrast, the T_1 state (denoted henceforth as ^{3}HCOH) is nonplanar with a dihedral angle of 103°, and it has a larger HCO angle, expanding from 106° in *cis*-HCOH(S_0) to 124° in T_1.[29] Likewise, the T_1 state of formaldehyde (^3H_2CO), which has been characterized both theoretically[15,22,29] and experimentally,[33−35] is nonplanar with a dihedral angle of ∼135°. Its vibrational levels are summarized in ref 35.

Our previous work has established that H_2CO and HCOH(D) can be prepared in the gas phase by photodissociation of CH_2OH(D) following excitation to the 3s, $3p_x$, and $3p_z$ Rydberg states.[10,11,36−38] Formaldehyde and hydroxymethylene are the main products of O−H and C−H bond breaking in CH_2OH, respectively. The lowest dissociation channels are[11,39]

$$CH_2OH \rightarrow H_2CO(\tilde{X}\ ^1A_1) + H$$
$$D_0 = 10\,160 \pm 70\ cm^{-1}\ (29 \pm 0.2\ kcal/mol) \quad (I)$$

$$CH_2OH \rightarrow \textit{trans}\text{-}HCOH(\tilde{X}\ ^1A') + H$$
$$D_0 = 28\,420 \pm 70\ cm^{-1}\ (81.2 \pm 0.2\ kcal/mol) \quad (II)$$

$$CH_2OH \rightarrow \textit{cis}\text{-}HCOH(\tilde{X}\ ^1A') + H$$
$$D_0 = 29\,970 \pm 70\ cm^{-1}\ (85.6 \pm 0.2\ kcal/mol) \quad (III)$$

Using the CH_2OD isotopolog, we have recorded H and D photofragment yield spectra as a function of excitation energy.[36,37] With 27 400−30 500 cm^{-1} (3s) photolysis, only O−D bond-breaking is observed, whereas at >30 500 cm^{-1} both D and H products are detected. The signal from the C−H bond fission channel increases monotonically with photolysis energy and reaches D:H ∼ 1 when exciting to the $3p_z$ state at >41 000 cm^{-1}.[10,38]

The product channels above are reached via conical intersections along the O−H and C−H coordinates.[40,41] Recently, we have demonstrated that upon excitation to the origin band of $3p_x$ (35 053 cm^{-1}) and above, the *cis* isomer of hydroxymethylene is preferred over the lower energy *trans* isomer.[11] Indeed, Yarkony predicted such a preference for photodissociation events that sample conical intersection seams along the C−H bond coordinate.[41]

In the present study, we turn our attention to excitation energies in the $3p_x$ and $3p_z$ states of the hydroxymethyl radical, where high vibrational levels and excited electronic states of the products are energetically accessible. By using CH_2OH and CH_2OD isotopologs, we are able to show that the triplet states of formaldehyde and hydroxymethylene are produced as minor dissociation channels. We note that this is the first experimental observation of the triplet state of hydroxymethylene. At yet higher energies, we obtain evidence for secondary dissociation of vibrationally excited hydroxymethylene.

In our previous study at these excitation energies,[10,38] we used the low-resolution core-sampling time-of-flight technique for H/D detection, which could not resolve internal states of the products. The present study is carried out at much higher kinetic energy (KE) resolution, which allows characterization of product vibrational and electronic states.

The technique we exploit, sliced velocity map imaging (SVMI), is an excellent tool for elucidating photodissociation dynamics and identifying product quantum states.[42,43] As pointed out previously, measuring velocity distributions directly, as done in SVMI, makes it possible to zoom-in on low-velocity regions of the distributions without the need to capture the full range of velocities (as must be done in full projection velocity map imaging).[42,44,45] This enhances resolution and signal-to-noise ratios and helps to identify minor products close to their energetic thresholds. SVMI is easy to implement for all photofragments except hydrogen, whose mass is too small for effective slicing.[46,47] Realizing that hydrogen photofragments carry most of the kinetic energy released in the photodissociation and therefore are useful reporters of quantum states of molecular cofragments, we have designed and implemented an SVMI arrangement optimized specifically for H fragments.[39,45,48] We have demonstrated vibrational resolution for H_2CO and HCOH(D) cofragments generated in CH_2OH(D) dissociation by measuring the kinetic energy distributions (KEDs) of H(D) products.[11,39]

II. EXPERIMENTAL DETAILS

The experimental arrangement for generating hyrodroxymethyl radicals in a molecular beam and detection of H(D) photofragments using SVMI was described in detail elsewhere,[39,45,48] and therefore only a brief description is given below.

CH_2OH radicals are produced in a quartz tube (length = 7 mm, i.d. = 1 mm) attached to a pulsed nozzle by the reactions $Cl_2 \rightarrow 2Cl$ and $CH_3OH + Cl \rightarrow CH_2OH + HCl$. Mixtures of CH_3OH (3%; Mallinckrodt Chemicals, 99.8% purity), Cl_2 (0.5%; Matheson AirGas, 99.5% purity), and He (Gilmore, Liquid−Air Company, 99.999% purity) are prepared in a glass bulb at 1.7 atm total pressure and are expanded into the source region of the vacuum chamber through a piezoelectrically driven pulsed-nozzle operating at 10 Hz. Cl_2 photodissociation is achieved with 355 nm radiation (∼12 mJ; third harmonic of Quanta-Ray GCR-11 Nd:YAG laser) focused with a cylindrical lens (f.l. = 15 cm) at the tip of the quartz tube. The desired isotopologs of CH_2OH are generated by selecting deuterated methanol precursors (CH_3OD; Aldrich 99.5 atom % D and CD_3OD; Aldrich 99.8 atom % D).

After passing through a skimmer (Beam Dynamics, orifice diameter = 1.0 mm), the molecular beam is intersected at right angles by two counterpropagating laser beams. The radicals are first excited by UV laser radiation (225−285 nm) from the frequency doubled output of the a dye laser (Continuum ND6000, Coumarin dyes) pumped by the third harmonic output of a pulsed Nd:YAG laser (Continuum, PL8000). Approximately 2 ns later H and D photofragments are probed by 1 + 1′ two-color REMPI via the Lyman-α transition. The required vacuum ultraviolet (VUV) laser radiation at ∼121.6 nm is generated by frequency tripling of ∼365 nm (2−3 mJ) radiation focused into a gas mixture of Kr:Ar 200:590 Torr in a metal cell. The VUV radiation is focused into the chamber using a MgF_2 lens (f.l. = 7.5 cm). The residual ∼365 nm radiation ionizes the excited H(D) fragments. The 365 nm radiation is generated by frequency doubling the output of a dye laser (Continuum, ND6000, LDS 722 dye) pumped with 532 nm laser radiation (2nd harmonic of a Nd:YAG laser; Continuum, NY-81C).

dx.doi.org/10.1021/jp505108k | J. Phys. Chem. A XXXX, XXX, XXX−XXX

$H^+(D^+)$ ions generated in the source region are accelerated through the flight tube toward a position sensitive detector (a phosphor screen coupled to a double-stack diameter = 40 mm microchannel plate; Galileo Electro-Optics 3040FM series). Image magnification is controlled by changing the voltage of the Einzel lens located in the field free region of the flight tube.[45,48] The degree of magnification is selected on the basis of the maximum H(D) fragment kinetic energy of interest. A digital video-camera (PixeLINK PL-B741F), located behind the phosphor screen of the detector, captures ion hit events produced in each laser shot, and the signal is transferred to a computer for further analysis. All SVMI images are recorded by tuning the H(D) detection laser through the Doppler profile of the H(D) fragment.

When operating in SVMI mode, fast gating of the detector (back plate of the MCP) is achieved by using a home-built high-voltage pulser (~5 ns fwhm, 2 kV peak).[45,48] To attain the desirable slice thickness (<10% of the whole ion cloud stretched to ~50 ns) and KE resolution, optimal voltage settings of the ion optics are selected by performing numerical ion trajectory simulations using the SIMION[49] program. However, when the products span a broad range of kinetic energies, the effective slice thickness varies within the image. For example, the effective slice thickness increases from 9.6% to 25% as the H-fragment kinetic energy decreases from 1.0 to 0.15 eV, which corresponds to a change in KE resolution, ΔKE/KE, from <2% to up to ~12% for the thick slices. The KE resolution of our instrument is characterized in SVMI measurements of O^+ products from O_2 photodissociation, which have a broad KE range.[48] The lower KE resolution at the lowest KEs does not hinder the determination of product channel onsets and in fact enables detection of low-KE minor products in the presence of other predominant product channels, as described below.

The center slice of the ion cloud is located by recording several slice images around the center and comparing them to select (i) the largest image radius and (ii) the sharpest ring structure—the two features indicative of the center slice. The optimal time delay between the detection laser pulse and the detector gating pulse is determined by using the above procedure. To maximize signal collection, images recorded at excitation energies above the $3p_z$-origin transition are acquired with excitation laser polarization parallel to the detector surface. H(D) fragments originating in $3s/3p_x$ excitation (recoil anisotropy parameter $\beta < 0$)[10] are imaged with excitation laser polarization perpendicular to the detector.

The sliced images are transformed from Cartesian to polar coordinates before further analysis. Slight image distortions due to inhomogeneous electric fields along the radial directions are corrected as described before.[45] Radial distribution plots of product intensities are obtained by integrating the signal at each radius in pixel space over 360°. The H/D distributions are then transformed from pixels to relevant domains (kinetic energy or velocity) by using the appropriate Jacobians, and they can be converted to center-of-mass KEDs by using momentum conservation.

Background signals originating from the detection laser are small compared to the pump−probe signal. Such background images are collected under identical experimental conditions and acquisition times in the absence of pump (excitation) laser radiation and are then subtracted from the pump−probe images before analysis. Images recorded by exciting to specific $3p_z$ vibronic levels include contributions from underlying $3s/3p_x$ states, whose absorptions are structureless. These background signals are estimated by acquiring images at laser frequencies slightly detuned from the $3p_z$ resonances (<100 cm^{-1}), and subtracted out from the on-resonance $3p_z$ images before plotting.

III. RESULTS AND DISCUSSION

Sliced H(D) photofragment images were recorded at several excitation energies of the $3p_x$ and $3p_z$ Rydberg states of CH_2OH and CH_2OD. Our investigation was focused on excitation energies near the energy onsets of (i) ^3H_2CO ($\tilde{a}\ ^3A_2$) and ^1H_2CO ($\tilde{A}\ ^1A_2$); (ii) ^3HCOD ($\tilde{a}\ ^3A''$); and (iii) secondary dissociation of vibrationally excited H_2CO and HCOH(D). The shaded areas in Figure 1 show excitation energies (E_{exc}) of

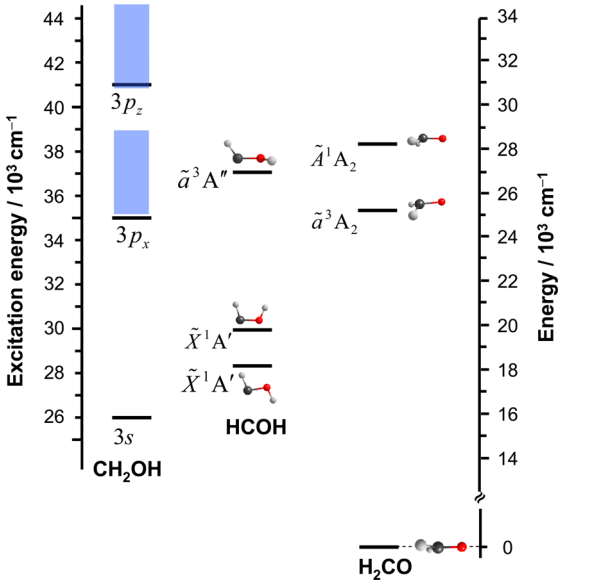

Figure 1. Energies of excited Rydberg states of CH_2OH are shown on the left scale. The shaded areas correspond to the excitation energies (E_{exc}) of the $3p_x$ and $3p_z$ states investigated in this work. The scale on the right shows the energies of singlet and triplet states of H_2CO and HCOH products relative to the ground state of H_2CO.

$CH_2OH(D)$ covered in the present study. We use CH_2OD to distinguish between the H_2CO and HCOD product channels by monitoring D and H photofragments, respectively.

III.A. Triplet States of Formaldehyde and Hydroxymethylene. The lowest excited electronic states of the products are the triplet states of formaldehyde and hydroxymethylene, which are separated by ~2000 cm^{-1} (Figure 1). Figure 2 shows H-fragment images and the corresponding radial velocity distributions recorded with CH_2OH precursor at excitation energies 35 053−36 036 cm^{-1}, which are in the proximity of the ^3H_2CO product threshold. The ion optics settings (ion acceleration and lens voltages) are optimized to "zoom-in" on H-fragments with KE < 8000 cm^{-1}. In other words, at these excitation energies H-fragments that correspond to ground-state H_2CO cofragments and have KEs above this value are not detected. We present the results as radial velocity distributions, rather than KER plots, because such plots give greater weight to low velocities, and thus are useful for identifying appearance thresholds of products that have low yields. The singlet−triplet energy gap in formaldehyde (ΔE_{S-T} = 25 194 cm^{-1})[33,35] and the dissociation energy of CH_2OH to generate ground-state H_2CO (10 160 cm^{-1})[39] are well

dx.doi.org/10.1021/jp505108k | J. Phys. Chem. A XXXX, XXX, XXX−XXX

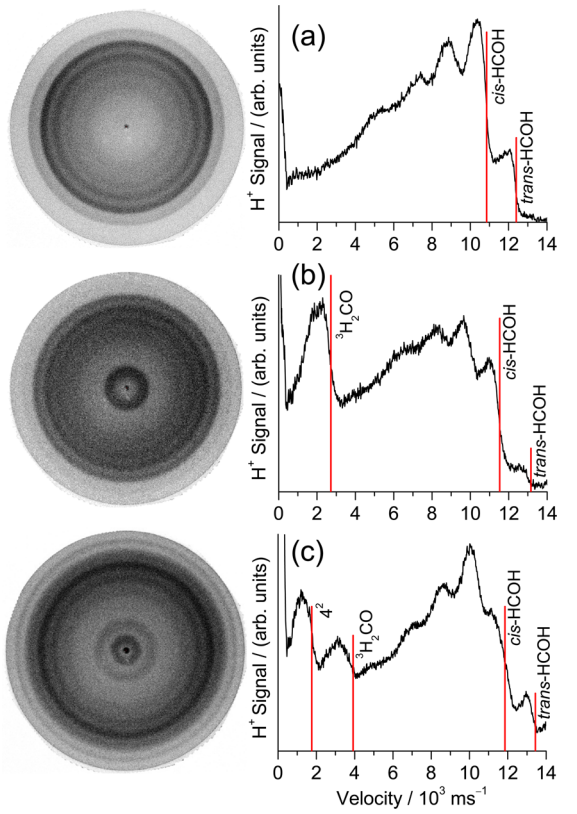

Figure 2. Left and right panels: SVMI images and the corresponding radial velocity distributions of H photofragments recorded at the following CH_2OH excitation energies ($3p_x$): (a) 35 053 cm^{-1}; (b) 35 714 cm^{-1}; (c) 36 036 cm^{-1}. Onsets of product states are indicated by red sticks. The images were obtained by zooming in on the low-velocity region, which is correlated mainly with HCOH products. The higher velocity region corresponding to H_2CO cofragments in the ground electronic state[11] is not shown. The peak at near-zero velocities is from hydrogen atom contamination.

established. These values allow us to determine that the energy threshold of ^3H_2CO with respect to the CH_2OH ground state is 35 354 cm^{-1}. The velocity distribution shown in Figure 2a was recorded at E_{exc} = 35 053 cm^{-1}, just below the ^3H_2CO onset, and it is correlated only with rovibrational levels of *cis*- and *trans*-HCOH cofragments in their ground electronic states.[11] The partially resolved peaks at higher velocities (>6000 ms^{-1}) correspond to the ground and low vibrational states of HCOH products.[11] As seen in Figure 2, the signal corresponding to higher rovibrational product levels (lower H velocities) is unresolved and its intensity decreases gradually with decreasing H fragment KE.

When E_{exc} is increased to 35 714 cm^{-1}, i.e., ~360 cm^{-1} above the expected ^3H_2CO threshold, the emergence of a new low-KE product peak is evident (Figure 2b). The energetic onset of this peak is at 25 243 ± 140 cm^{-1} above the formaldehyde ground state, in good agreement with ΔE_{S-T}.[33,35] The two lowest vibrational levels of triplet-H_2CO are the fundamental and first overtone of the inversion mode (ν_4), which are at 36 and 538 cm^{-1} above the zero-point energy (ZPE).[35] Due to significant rotational excitation in the ground vibrational level and 4^1, these two energy levels are not resolved. However, with a further increase in excitation energy, clear emergence of a second peak at energy corresponding to the 4^2 vibrational level (538 cm^{-1}) is observed and is labeled by a stick in Figure 2c. With a further increase in excitation energy, the vibrational levels get broadened by increased rotational excitation and blend into the broad background of high rovibrational levels of ground-state products.

The assignment of the peaks to ^3H_2CO is strengthened by carrying out corresponding measurements with CH_2OD. By detecting D-fragments, we probe only the product distribution in the formaldehyde cofragment and eliminate signals from hydroxymethylene. Figure 3 shows the "zoomed-in" portion of

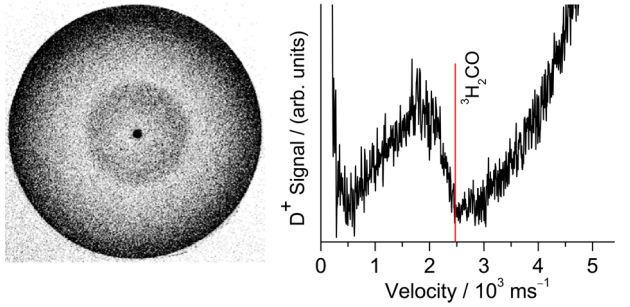

Figure 3. Image and radial D-fragment velocity distribution from CH_2OD excitation recorded at E_{exc} = 36 563 cm^{-1}. The low-velocity peak corresponds to ^3H_2CO. The distribution was obtained by zooming in on the 0−5000 ms^{-1} velocity region.

the D-fragment velocity distribution obtained by exciting CH_2OD at 36 563 cm^{-1}. This image is acquired under SVMI conditions that produce thicker slices (25% slice thickness) in the low-KE region. Nevertheless, the peak in the low-velocity part is clear, and its appearance threshold conforms with the formation of ^3H_2CO. The rising signal intensity toward higher velocities is associated with rovibrational levels of H_2CO in the ground electronic states, as discussed elsewhere.[11] The onset of ^3H_2CO is observed at 36 017 ± 70 cm^{-1} with respect to CH_2OD. After taking into account the harmonic ZPE difference between CH_2OD and CH_2OH ($E^{ZPE}_{CH_2OD} - E^{ZPE}_{CH_2OH}$= 671 cm^{-1}),[50] we estimate the formaldehyde S−T gap to be 25 186 ± 140 cm^{-1}. Within experimental error this value agrees well with previous spectroscopic measurements.[33−35] The onset of the 4^2 vibration level is observed at slightly higher excitation energy (E_{exc} = 36 630 cm^{-1}).

Our observations imply that the CH_2 wag mode of ^3H_2CO is populated. This can be rationalized by considering the geometries of reactants and products. The differences between the equilibrium molecular geometries of ground-state CH_2OH, CH_2OH ($3p_x$), and the ^3H_2CO product are significant. The geometry of CH_2OH ($3p_x$) resembles that of the CH_2OH^+ ion, which is planar (C_s symmetry), whereas ground-state CH_2OH is nonplanar (C_1 symmetry). ^3H_2CO has a pyramidal geometry around the carbon center (Figure 1). This implies that a major geometry change occurs along the CH_2 wag (inversion) coordinate, in accordance with a pyramidal geometry with a large out-of-plane angle. It is therefore likely that O−H bond fission occurs in the nonplanar geometry, and the CH_2 wag levels of CH_2OD convert to ν_4 excitation in ^3H_2CO. Analogous geometry change considerations were used to explain the observation of C−O stretch and in-plane CH_2 scissors vibrational levels in the planar $H_2CO(S_0)$ product.[11]

We note that the yield of ^3H_2CO is much lower in photodissociation of CH_2OD than CH_2OH. Attempts to record D-fragment images by exciting CD_2OD failed to reveal the ^3D_2CO product onset above the background of ground-

dx.doi.org/10.1021/jp505108k | J. Phys. Chem. A XXXX, XXX, XXX−XXX

state formaldehyde. We conclude that the yield of triplet formaldehyde depends sensitively on the isotopolog precursor used and decreases with increasing degree of deuteration. This may reflect the dependence of the conical intersection seams that lead to triplet formaldehyde formation on the degree of deuteration of the hydroxymethyl precursor.

Encouraged by our ability to detect the onset of the minor ^3H_2CO product, we searched for the triplet state of hydroxymethylene, which lies ~2000 cm^{-1} higher in energy but has never been detected experimentally. Our search has been guided by the available theoretical predictions, which place ΔE_{S-T} of HCOH around 25 kcal/mol (~8740 cm^{-1}).[22,25,28,29,31] To monitor only the C−H bond breaking channel, we used CH_2OD as a precursor and measured the velocity distributions of H products correlated with HCOD cofragments. Although the isotopic difference between the calculated ΔE_{S-T} for HCOH and our measurements for HCOD was not taken into account, this difference is expected to be small compared with the uncertainties in the experimental measurements described below.

Figure 4 shows overlaid velocity distributions recorded at CH_2OD excitation energies 37 106 and 37 313 cm^{-1},

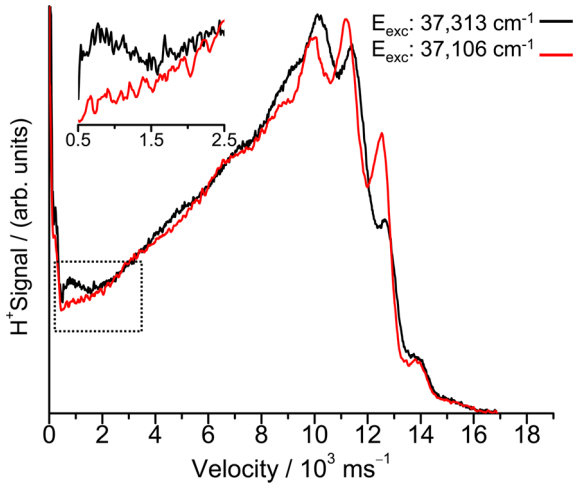

Figure 4. H-fragment radial velocity distributions obtained with excitation energies 37 106 cm^{-1} (red) and 37 313 cm^{-1} (black) overlaid to demonstrate the appearance of a new feature assigned as the onset of ^{3}HCOD. The inset shows a magnified plot of the low-velocity region.

respectively, near the threshold for ^{3}HCOD formation. In excitation at 37 106 cm^{-1}, which is 9132 cm^{-1} above the threshold for production of ground-state *trans*-HCOD, the H^+ signal intensity decreases gradually with decreasing velocity. The H-fragment velocity distribution obtained at slightly higher excitation energy (37 313 cm^{-1}) shows a very small but reproducible new feature emerging at the lowest velocities above the background of ground-state HCOD fragments. The high-velocity part remains nearly unchanged with only small intensity fluctuations. Comparing the two plots, we assign the new feature as the predicted onset of ^{3}HCOD. From Figure 4 we determine ΔE_{S-T} = 9230 ± 400 cm^{-1} (26.39 ± 1.1 kcal/mol) for HCOD. However, determining the exact threshold is challenging because of the small size and large width of the new feature, the large background signal, and our inability to observe additional distinct structures in the velocity distributions at higher energies. Recalling that HCOD products in their ground electronic state are born with a high degree of rovibrational excitation,[11] it is likely that the same is true for ^{3}HCOD. Thus, when the dissociation energy is increased, the signal associated with the triplet-state blends into the high density of rovibrational levels of the ground state. We therefore consider the assignment of the triplet state of HCOD as tentative.

The stability of ^{3}HCOD is unknown. Previous results in an Ar matrix showed that ground-state HCOH converts to H_2CO by tunneling, but HCOD is stable for a long time. However, this situation may change for ^{3}HCOD, which is ~9200 cm^{-1} higher in energy and is close to the dissociation energy to CO + H_2. This state may isomerize faster to HDCO by tunneling or undergo efficient coupling to the ground state.

The excited singlet state of formaldehyde is located 28 188 cm^{-1} above its ground state or 2994 cm^{-1} above the triplet state (Figure 1).[33,35] We have searched for this product near its energetic onset by recording D-fragment images from CH_2OD photodissociation. No new distinct product channel openings were observed above the broad background of high rovibrational states of ground and triplet-state H_2CO fragments. Thus, if H_2CO (S_1) is produced at all, its yield must be very small.

III.B. Vibrational Excitation and Dissociation of HCOD Products. In this section we report on the production of highly vibrationally excited HCOD. In previous work we showed that as the excitation energy of the $CH_2OH(D)$ precursor increased, the internal energy of the molecular products increased as well;[38] however, the KE resolution of our instrument was low. With SMVI we achieved vibrational level resolution in the formaldehyde and hydroxymethylene products,[11] and therefore we extended the measurements to excitation energies that reached up to and beyond the dissociation threshold of the H_2CO and HCOH(D) products. We reported before that at excitation energies >40 000 cm^{-1}, the total D and H yields were similar.[38] We also showed that with excitation of CH_2OD to higher vibronic levels of $3p_z$, a new, low-KE feature appeared in the H and D fragment KEDs, whose widths increased with increasing excitation energy.[38] The appearance thresholds of these H/D fragments coincided with the dissociation energy of formaldehyde to H + HCO.[38,51] The question whether formaldehyde or hydroxymethylene (or both) was the source of the secondary dissociation of products remained unresolved.

Figures 5 and 6 display H and D KER plots obtained by SVMI following excitation of CH_2OD to the 0_0^0, 6_0^1, and 6_0^2 transitions of $3p_z$. The D-fragment KEDs are correlated with H_2CO cofragments, except for the small peak at low KE, which originates in secondary dissociation of HCOD.[38] The H-photofragment KEDs, on the other hand, are correlated with HCOD cofragments, and their partially resolved peaks reflect vibrational excitation in HCOD. The increased signals at the lowest KEs in the 6_0^1 and 6_0^2 plots correspond to H fragments generated by secondary dissociation of either "hot" HCOD or H_2CO products (or both). As shown before,[38] when exciting to the $3p_z$ origin band, which is right at the threshold for secondary dissociation, the low-KE peaks are absent. Low-KE peaks have been detected also with excitation to other $3p_z$ bands between the 0_0^0 and 6_0^2 bands.[38] Both the previous and the present studies show that as the excitation energy increases, the secondary dissociation peak broadens and increases in integrated intensity, but its energy onset (shown by sticks in Figures 5 and 6) always corresponds to the H(D) + HCO channel threshold.

dx.doi.org/10.1021/jp505108k | J. Phys. Chem. A XXXX, XXX, XXX−XXX

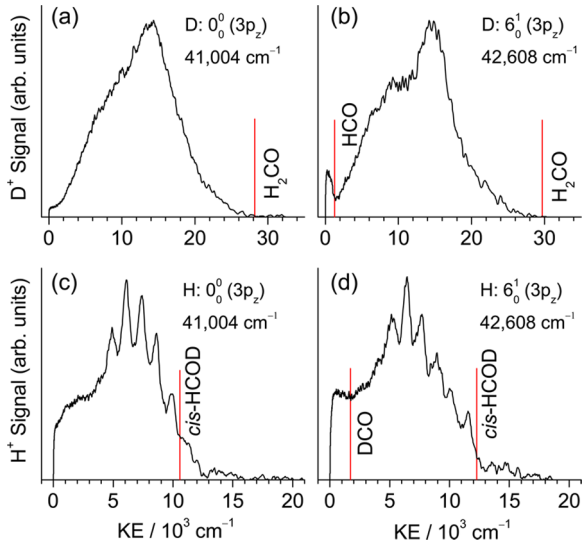

Figure 5. H- and D-fragment KER plots obtained by monitoring D^+ (upper panels) and H^+ (lower panels) following $3p_z$ excitation of CH_2OD to the (a, c) 0_0^0 (E_{exc} = 41 004 cm^{-1}) and (b, d) 6_0^1 (E_{exc} = 42 608 cm^{-1}) bands. The H-fragment KER plots were obtained by zooming in on the 0−20 000 cm^{-1} KE region to enhance resolution. Sticks in each panel indicate the KE onsets associated with H_2CO, *cis*-HCOD, and the appearance of H and D from secondary dissociation. See the text for details.

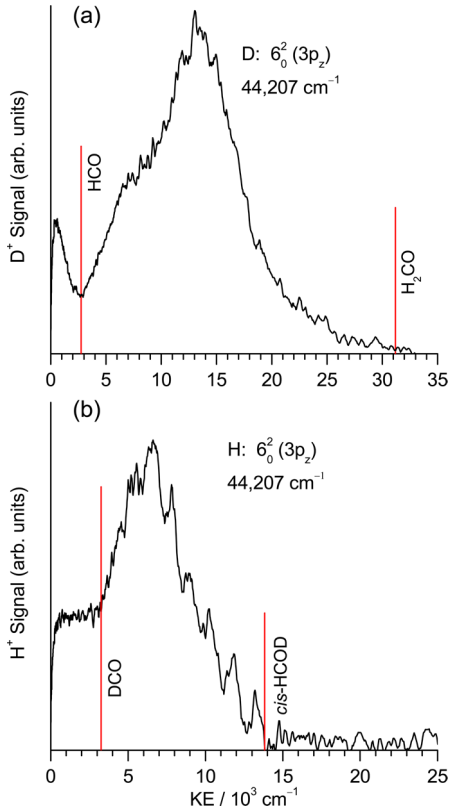

Figure 6. H- and D-fragment KER plots obtained by monitoring D^+ (upper panel) and H^+ (lower panel) following $3p_z$ excitation of CH_2OD to the 6_0^2 band (E_{exc} = 44 207 cm^{-1}). The H- and D-fragment KER plots were obtained by recording the entire allowed KE range. Sticks in each panel indicate the KE onsets associated with H_2CO, *cis*-HCOD, and H and D from secondary dissociation. See the text for details.

With the higher resolution afforded by SVMI, better analysis of the H and D KEDs is now possible. The D-fragment KED recorded at excitation energy below the threshold of secondary dissociation shows that only a very small fraction of the H_2CO products are born with the high internal energies required for secondary dissociation, and this fraction does not appear to increase at higher excitation energies. Therefore, H_2CO is not an important source of H fragments. In contrast, the H-fragment KEDs show that a significant fraction of HCOD cofragments possesses sufficient internal energies to dissociate to H(D) + D(H)CO at high excitation energies. Thus, HCOD is the only source of the observed secondary D atoms and the main source of secondary H fragments. We find that the yields of the slow H and D secondary products are comparable, and we conclude that they are generated predominantly by dissociation of vibrationally excited HCOD. This is the first report of the dissociation of hydroxymethylene, and we propose that the major dissociation pathway involves isomerization to HDCO followed by dissociation.

As discussed in section I, high-quality PESs now exist for the H_2CO/HCOH system. They include the ground state of formaldehyde and hydroxymethylene, as well as formaldehyde dissociation to H_2 + CO and H + HCO.[21,23,24,52] The T_1 and S_1 states of the two tautomers and their couplings to the S_0 state of formaldehyde have been characterized as well.[22−24] It is established by theory and experiment that the barrierless dissociation threshold of H_2CO to H + HCO lies 30 328 cm^{-1} above the H_2CO ZPE.[21,51] This energy is higher than the dissociation barrier of H_2CO to H_2 + CO (27 720 cm^{-1}),[53] the isomerization barrier of H_2CO to *trans*-HCOH (28 540 cm^{-1})[6], the *trans*-HCOH to *cis*-HCOH isomerization barrier (27 526 cm^{-1}),[6] and the T_1 levels of H_2CO (25 194 cm^{-1})[33,35] and HCOH (27 281 cm^{-1})[22]—all relative to the H_2CO ground state (including ZPE). The relevant states and barriers are shown schematically in Figure 7, which illustrates that it is energetically possible to reach H + HCO from HCOH via isomerization to H_2CO. Small changes due to ZPE differences need to be made for HCOD, but the order of states does not change.

In contrast to the wealth of calculations available on dissociation from the H_2CO global minimum, relatively little is known about the dissociation dynamics of HCOH. Reid et al. examined the dissociation of HCOH to H + HCO but did not include isomerization to formaldehyde.[54] They compared calculations for HCOH performed with CAS(10 10), CAS(8 8), and MRCI, using the cc-pVDZ basis set, and reported that the minima and barriers depended sensitively on the method used. Nevertheless, their analysis provides qualitative insights into the nature of the electronic states along the O−H reaction coordinate. They find an avoided crossing along O−H between the diabatic S_0 and S_1 states of *cis*- and *trans*-HCOH, which changes the electronic character of the adiabatic S_0 state at fairly short O−H separations (<2 Å). As a result of this avoided crossing, there can be either a small barrier (for the *trans* isomer) or a shelf-like region (for the *cis* isomer) along the O−H coordinate. In the language of transition-state theory this means that the transition states associated with dissociation of HCOH to H + HCO are much tighter than the loose transition state associated with the barrierless dissociation of H_2CO to H + HCO, which does not require a change in electronic character. The substantial electronic reorganization required for HCOH along the O−H coordinate can create a bottleneck to direct dissociation via this channel, which enables the

dx.doi.org/10.1021/jp505108k | J. Phys. Chem. A XXXX, XXX, XXX−XXX

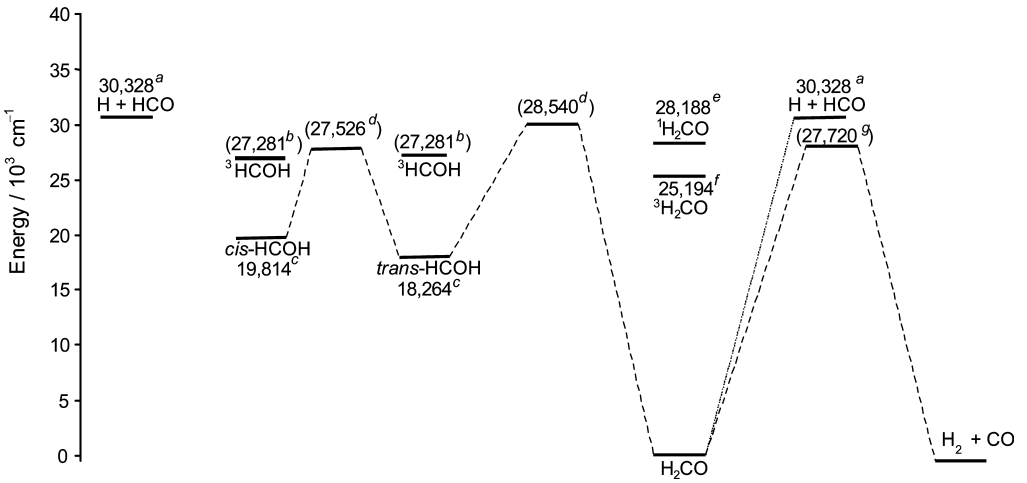

Figure 7. Schematic energy diagram showing relevant states and barrier energies (cm^{-1}) for H_2CO, HCOH, and their dissociation to H + HCO and H_2 + CO. Theoretical energy values (ZPE corrected) relative to the ground state of H_2CO are given in parentheses. Corresponding references: *a*, ref 51; *b*, ref 22; *c*, ref 11; *d*, ref 6 (similar values given also in ref 21); *e*, refs 34 and 35; *f*, ref 34; *g*, ref 53.

dominance of the isomerization channel. This isomerization mechanism explains the observation of comparable yields of secondary H and D fragments, as seen in Figures 5 and 6.

Hopefully our experimental results would inspire additional theoretical work on the H_2CO/HCOH PES that would include trajectory calculations initiated from the global minimum of HCOH. Up to now most of the trajectory calculations started in the H_2CO well. It is worth noting that in one calculation the trajectories were initiated at the T_1/S_0 minimum energy crossing configuration.[55] This crossing occurs at nuclear configurations similar to the transition state separating the ground-state *cis*- and *trans*-HCOH isomers. Trajectories were run at total energies of 35 000−38 000 cm^{-1} above the global H_2CO minimum, starting from different points corresponding to the *cis*- and *trans*-T_1/S_0 crossings. Shepler et al. report that trajectories terminating in CO + H_2 products sample the *cis*- and *trans*-HCOH wells before finding the much deeper H_2CO well, from which they eventually proceed to products. Regarding the H + HCO channel, they find that when including ZPE constraints, only ∼6% of the HCO fragments are produced from the HCOH well, while the majority dissociate via H_2CO. It appears, therefore, that the existence of the deep formaldehyde well guides the trajectories along this route. Finally, in regard to the CO + H_2 channel we note that we have already reported observation of CO products in $v = 0$ and 1 in dissociation of hydroxymethyl via the $3p_z$ state at energies >33 000 cm^{-1} above the H_2CO minimum.[38] These products can originate in secondary dissociation of formaldehyde either via a direct route or after HCOD isomerization. Determination of the CO rovibrational-state distribution might shed more light on the mechanism, though it is experimentally quite challenging.

The H-fragment KEDs obtained by SVMI following excitation to $3p_z$ show distinct peaks correlated with vibrational levels of *cis*-HCOD. It is noteworthy that these peaks are better resolved than in the corresponding KEDs obtained following 3s and $3p_x$ excitation.[11] To enhance the KE resolution, the H-fragment KEDs in Figure 5 were obtained by "zoomed in" SVMI settings to record only fragments with KE < 20 000 cm^{-1} (the total available KE for the formaldehyde product is >30 000 cm^{-1}). They were converted to center-of-mass KEDs to fit them with vibrational levels of *cis*-HCOD. The calculated vibrational frequencies of *cis*-HCOD are 847, 921, 1288, 1414, 2516, and 2584 cm^{-1}.[8] We obtain reasonable fits to the HCOD peaks shown in Figures 5 and 6 by using the four highest frequency vibrations, including overtones and combination bands. It appears that the CO-stretch and in-plane bend modes (1288 and 1414 cm^{-1}, respectively) provide the major excitations, though some contributions from the C−H and O−D stretch modes cannot be excluded. However, the observed peaks are quite broad and the fits are not unique, especially because rotational excitation may shift the peaks. Examples of fits are given in the Supporting Information. We note, however, that the peaks remain quite distinct even at excitation energies close to the isomerization and dissociation barriers of HCOD. For example the H-fragment KED shown in Figure 6, which was obtained at lower KE resolution (no "zooming in" on the HCOD region), exhibits distinct vibrational structures that extend close to ∼10 000 cm^{-1} above the *cis* isomer ground state, i.e., near the dissociation and isomerization barriers.

The present SVMI results allow us to reassess the dissociation energy for CH_2OD → *cis*-HCOD + H. Taking into account uncertainties in fragment rotational energy and checking for consistency with ZPE changes between the fully hydrogenated and partially deuterated reactants and products, our current best estimate is 29 534 ± 200 cm^{-1}. This value supersedes our previous value of 29 945 cm^{-1}. The corresponding value for CH_2OD → *trans*-HCOD + H is lower by 1560 cm^{-1}.

III.C. Implications to Conical Intersections in CH_2OH-(D). Finally, we comment on the effect of conical intersections leading to dissociation of $CH_2OH(D)$ on fragments' state distributions. About a decade ago, Yarkony carried out conical intersection calculations on the hydroxymethyl radical and identified conical intersection seams along the O−H and C−H coordinates following excitation to the 3s and $3p_x$ states.[40,41] He predicted that in conical intersections from the 3s state, formaldehyde products will have high translational energies and fairly low internal energies but a small fraction would sample the global minimum and would have a broad, statistical-like, internal energy distribution. He also predicted that *cis*- rather than *trans*-HCOH would be the predominant hydroxymethylene product. These predictions were confirmed in our

dx.doi.org/10.1021/jp505108k | J. Phys. Chem. A XXXX, XXX, XXX−XXX

previous work,[11] except that we found that the situation regarding HCOH production was more complicated. In excitation to the 3s state, the yield of HCOH(D) was fairly small, and because of its high rotational excitation it was impossible to distinguish between the *trans* and *cis* isomers. However, upon excitation to the $3p_x$ origin band, the rotational excitation in the HCOH(D) isomers was reduced considerably and vibrational structure was observed. This allowed us to show that the *cis* isomer was preferentially produced and its relative population increased with increasing excitation energy. Nonetheless, the rotational excitation was still fairly high and obscured vibrational structure at high internal HCOH(D) energies.

Our present work shows that another abrupt reduction in the HCOH(D) rotational excitation occurs upon excitation to the $3p_z$ state, which in turn allows the observation of distinct vibrational structure in the HCOD fragment even at high internal energies. The vibrational excitation spans the full range of allowed internal energies, reaching up to and above the dissociation limit of HCOH(D). The loss of structure observed at very high internal energies can signify either increasing IVR leading to a higher density of states and/or a greater contribution of ^{3}HCOH(D) at >7670 cm^{-1} above the ground vibrational state of *cis*-HCOH(D).

As reported previously, the H/D photofragment yield spectra of $CH_2OH(D)$ show that underlying the sharp $3p_z$ vibronic bands there is a structureless background of absorption to 3s and $3p_x$. This gives us an opportunity to observe the differences between the HCOD rovibrational-state distributions at similar energies. Figure 8 presents a comparison of the H-fragment

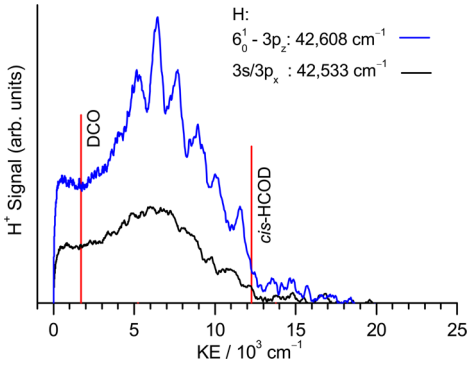

Figure 8. Comparison of *cis*-HCOD internal-state distributions obtained via $3p_z$ excitation of CH_2OD to the 6_0^1 band (E_{exc} = 42 608 cm^{-1}), and by excitation to the 3s/$3p_x$ underlying background (E_{exc} = 42 553 cm^{-1}). The background contribution is already subtracted in the 6_0^1 plot. Sticks indicate the KE onsets associated with *cis*-HCOD and H from secondary dissociation. Note the more prominent vibrational structures in the 6_0^1 plot than in the 3s/$3p_x$ plot.

KEDs obtained at the 6_0^1 peak of $3p_z$ (after background subtraction) and the one recorded ~70 cm^{-1} to the red, which derives from 3s/$3p_x$ continuous absorptions. Indeed, the latter displays a much greater rotational excitation that obscures much of the vibrational structure.

These results suggest that the dissociation dynamics is not controlled solely by the 3s PES and its coupling to the ground state; rather, different dynamics ensues by going through different conical intersections. In all cases the dissociation is fast; even the $3p_z$ state, which shows fairly sharp vibronic structure, has a lifetime <0.5 ps.[56] Yet, the resulting dynamics is quite different. It is not clear whether the $3p_z$ and $3p_x$ states couple directly to the ground state, or whether sequential conical intersections link the upper states to the ground state and guide the dissociating flux in ways that affects significantly the rotational excitation. New theoretical calculations on a global PES that includes all the participating Rydberg states as well as wave packet propagation may shed further light on the dissociation mechanisms.

IV. SUMMARY AND CONCLUSIONS

The SVMI results presented above provide additional information on the elusive carbene, hydroxymethylene, while also revealing fingerprints of the conical intersections that control the photodissociation dynamics of the hydroxymethyl radical precursor following excitation to its lowest lying Rydberg states. The main photodissociation products of O−H(D) and C−H bond breaking are formaldehyde and hydroxymethylene, respectively, and their internal energies are estimated from the KEDs of H and D cofragments.

The HCOD fragment generated by excitation of CH_2OD to the $3p_x$ and $3p_z$ Rydberg states is mainly the *cis* isomer that lies ~1550 cm^{-1} above the *trans* isomer. It is born with high rotational and vibrational excitation that encompasses the full range of allowed energies. Its internal excitation depends on the excited Rydberg state of CH_2OD. Specifically, the rotational excitation of HCOD is much lower when it is accessed via the higher-lying $3p_z$ state than via the $3p_x$ state. The lower rotational excitation allows characterization of the excited vibrational modes, and we find that the CO-stretch and in-plane bending modes carry much of the HCOD vibrational excitation. Distinct vibrational structure can be observed even at energies as high as ~9000 cm^{-1} above the *cis* isomer ground state, quite close to the dissociation threshold to D + HCO and the barrier to isomerization to formaldehyde. When the internal energy of HCOD exceeds its dissociation threshold to D + HCO, slow D and H fragments from secondary dissociation are observed. As the yields of these H and D fragments are comparable, we propose that isomerization to HDCO precedes dissociation. We also obtain evidence for production of HCOD in the triplet state at ~9200 cm^{-1} above *trans*-HCOD, a slightly higher value (~480 cm^{-1}) compared to the calculated S−T gap for HCOH. The triplet peak is small and due to its high level of rovibrational excitation it blends into the large background of rovibrational levels of the ground state at higher excitation energies. Therefore, we consider this assignment tentative. We note that so far photodissociation of CH_2OD is the only way to produce and characterize the *cis*-HCOH(D) isomer.

The KEDs of H- and D-photofragment obtained in photodissociation of CH_2OH and CH_2OD allow us also to further characterize the formaldehyde product, which is generated by O−H bond breaking. A large fraction of the available energy is released in translation, although the extent of internal excitation increases and its range broadens with increasing dissociation energy. In addition, we are also able to identify clearly the formation threshold of the triplet state of formaldehyde, even though it is a minor channel, and observe distinct peaks in the H/D KEDs that are correlated with its ground state and excited ν_4 vibrations. The triplet-state onset agrees well with the spectroscopically determined S−T gap in formaldehyde. The relative yield of triplet formaldehyde decreases with increasing deuteration of the precursor, suggesting subtle changes in the conical intersection seams that govern its formation.

dx.doi.org/10.1021/jp505108k | J. Phys. Chem. A XXXX, XXX, XXX−XXX

The rotational, vibrational, and electronic excitations in the formaldehyde and hydroxymethylene products depend on the excited Rydberg state of the hydroxymethyl precursor and the degree of deuteration, and therefore they provide fingerprints of the conical intersection seams that lead from the precursor's Rydberg states to products. We hope that the detailed results presented here would inspire additional theoretical calculations on the production of hydroxymethylene and its subsequent dissociation.

■ ASSOCIATED CONTENT

Ⓢ Supporting Information

Vibrational structure fittings of the H-fragment kinetic energy distribution recorded at CH_2OD excitation energy 41 004 cm^{-1} ($3p_z$ origin). List of fundamentals for *cis*-HCOD. This material is available free of charge via the Internet at http://pubs.acs.org.

■ AUTHOR INFORMATION

Corresponding Author

*H. Reisler: e-mail, reisler@usc.edu.

Notes

The authors declare no competing financial interest.

■ ACKNOWLEDGMENTS

Support by the U.S. Department of Energy, Basic Energy Sciences, Grant No. DE-FG02-05ER15629, is gratefully acknowledged.

■ REFERENCES

(1) Baly, E. C. C.; Heilbron, I. M.; Hudson, D. P. CXXX.—Photocatalysis. Part II. The Photosynthesis of Nitrogen Compounds from Nitrates and Carbon Dioxide. *J. Chem. Soc., Trans.* **1922**, *121*, 1078−1088.

(2) Lucchese, R. R.; Schaefer, H. F., III. Metal-Carbene Complexes and the Possible Role of Hydroxycarbene in Formaldehyde Laser Photochemistry. *J. Am. Chem. Soc.* **1978**, *100*, 298−299.

(3) Bowman, J. M.; Shepler, B. C. Roaming Radicals. *Annu. Rev. Phys. Chem.* **2011**, *62*, 531−553.

(4) Moore, C. B.; Weisshaar, J. C. Formaldehyde Photochemistry. *Annu. Rev. Phys. Chem.* **1983**, *34*, 525−555.

(5) Suits, A. G.; Chambreau, S. D.; Lahankar, S. A. State-Correlated DC Slice Imaging of Formaldehyde Photodissociation: Roaming Atoms and Multichannel Branching. *Int. Rev. Phys. Chem.* **2007**, *26*, 585−607.

(6) Schreiner, P. R.; Reisenauer, H. P.; Pickard, F. C.; Simmonett, A. C.; Allen, W. D.; Matyus, E.; Csaszar, A. G. Capture of Hydroxymethylene and its Fast Disappearance Through Tunnelling. *Nature* **2008**, *453*, 906−909.

(7) Leavitt, C. M.; Moradi, C. P.; Stanton, J. F.; Douberly, G. E. Helium Nanodroplet Isolation and Rovibrational Spectroscopy of Hydroxymethylene. *J. Chem. Phys.* **2014**, *140*, 171102.

(8) Koziol, L.; Wang, Y. M.; Braams, B. J.; Bowman, J. M.; Krylov, A. I. The Theoretical Prediction of Infrared Spectra of Trans- and Cis-Hydroxycarbene Calculated Using Full Dimensional Ab Initio Potential Energy and Dipole Moment Surfaces. *J. Chem. Phys.* **2008**, *128*, 204310.

(9) Bucher, G. Hydroxycarbene: Watching a Molecular Mole at Work. *Angew. Chem., Int. Ed.* **2008**, *47*, 6957−6958.

(10) Feng, L.; Demyanenko, A. V.; Reisler, H. Competitive C-H and O-D Bond Fission Channels in the UV Photodissociation of the Deuterated Hydroxymethyl Radical CH_2OD. *J. Chem. Phys.* **2004**, *120*, 6524−6530.

(11) Rodrigo, C. P.; Zhou, C.; Reisler, H. Accessing Multiple Conical Intersections in the 3s and $3p_x$ Photodissociation of the Hydroxymethyl Radical. *J. Phys. Chem. A* **2013**, *117*, 12049−12059.

(12) Yeung, E. S.; Moore, C. B. Photochemistry of Single Vibronic Levels of Formaldehyde. *J. Chem. Phys.* **1973**, *58*, 3988−3998.

(13) Houston, P. L.; Moore, C. B. Formaldehyde Photochemistry: Appearance Rate, Vibrational Relaxation, and Energy Distribution of the CO Product. *J. Chem. Phys.* **1976**, *65*, 757−770.

(14) Goddard, J. D.; Yamaguchi, Y.; Schaefer, H. F., III. Features of the H_2CO Potential Energy Hypersurface Pertinent to Formaldehyde Photodissociation. *J. Chem. Phys.* **1981**, *75*, 3459−3465.

(15) Goddard, J. D., III; Schaefer, H. F., III. The Photodissociation of Formaldehyde: Potential Energy Surface Features. *J. Chem. Phys.* **1979**, *70*, 5117−5134.

(16) Osamura, Y.; Goddard, J. D.; Schaefer, H. F., III; Kim, K. S. Near Degenerate Rearrangement Between the Radical Cations of Formaldehyde and Hydroxymethylene. *J. Chem. Phys.* **1981**, *74*, 617−621.

(17) Lahankar, S. A.; Chambreau, S. D.; Townsend, D.; Suits, F.; Farnum, J.; Zhang, X. B.; Bowman, J. M.; Suits, A. G. The Roaming Atom Pathway in Formaldehyde Decomposition. *J. Chem. Phys.* **2006**, *125*, 44303.

(18) Lahankar, S. A.; Chambreau, S. D.; Zhang, X. B.; Bowman, J. M.; Suits, A. G. Energy Dependence of the Roaming Atom Pathway in Formaldehyde Decomposition. *J. Chem. Phys.* **2007**, *126*, 44314.

(19) Lahankar, S. A.; Goncharov, V.; Suits, F.; Farnum, J. D.; Bowman, J. M.; Suits, A. G. Further Aspects of the Roaming Mechanism in Formaldehyde Dissociation. *Chem. Phys.* **2008**, *347*, 288−299.

(20) Suits, A. G. Roaming Atoms and Radicals: A New Mechanism in Molecular Dissociation. *Acc. Chem. Res.* **2008**, *41*, 873−881.

(21) Zhang, X.; Zou, S.; Harding, L. B.; Bowman, J. M. A Global ab Initio Potential Energy Surface for Formaldehyde. *J. Phys. Chem. A* **2004**, *108*, 8980−8986.

(22) Zhang, P.; Maeda, S.; Morokuma, K.; Braams, B. J. Photochemical Reactions of the Low-lying Excited States of Formaldehyde: T_1/S_0 Intersystem Crossings, Characteristics of the S_1 and T_1 Potential Energy Surfaces, and a Global T_1 Potential Energy Surface. *J. Chem. Phys.* **2009**, *130*, 114304.

(23) Rheinecker, J. L.; Zhang, X.; Bowman, J. M. Quasiclassical Trajectory Studies of the Dynamics of H_2CO on a Global Ab Initio-based Potential Energy Surface. *Mol. Phys.* **2005**, *103*, 1067−1074.

(24) Fu, B.; Shepler, B. C.; Bowman, J. M. Three-State Trajectory Surface Hopping Studies of the Photodissociation Dynamics of Formaldehyde on ab Initio Potential Energy Surfaces. *J. Am. Chem. Soc.* **2013**, *133*, 7957−7968.

(25) Gronert, S.; Keeffe, J. R.; More O'Ferrall, R. A. Stabilities of Carbenes: Independent Measures for Singlets and Triplets. *J. Am. Chem. Soc.* **2011**, *133*, 3381−3389.

(26) Hoffmann, M. R.; Schaefer, H. F., III. Hydroxycarbene (HCOH) and Protonated Formaldehyde - Two Potentially Observable Interstellar Molecules. *Astrophys. J.* **1981**, *249*, 563−565.

(27) Hwanga, D.-Y.; Mebela, A. M.; Wanga, B.-C. Ab Initio Study of the Addition of Atomic Carbon with Water. *Chem. Phys.* **1999**, *244*, 143−149.

(28) Kiselev, V. G.; Swinnen, S.; Nguyen, V. S.; Gritsan, N. P.; Nguyen, M. T. Fast Reactions of Hydroxycarbenes: Tunneling Effect versus Bimolecular Processes. *J. Phys. Chem. A* **2010**, *114*, 5573−5579.

(29) Matus, M. H.; Nguyen, M. T.; Dixon, D. A. Heats of Formation and Singlet−Triplet Separations of Hydroxymethylene and 1-Hydroxyethylidene. *J. Phys. Chem. A* **2006**, *110*, 8864−8871.

(30) Schreiner, P. R.; Reisenauer, H. P. The "Non-Reaction" of Ground-State Triplet Carbon Atoms with Water Revisited. *ChemPhysChem* **2006**, *7*, 880−885.

(31) Shen, J.; Fang, T.; Li, S. Singlet-triplet Gaps in Substituted Carbenes Predicted from Block-correlated Coupled Cluster Method. *Sci. China, Ser. B Chem.* **2008**, *51*, 1197−1202.

(32) Lessard, C. R.; Moule, D. C. The Assignment of the Rydberg Transitions in the Electronic Absorption Spectrum of Formaldehyde. *J. Chem. Phys.* **1977**, *66*, 3908−3916.

(33) Herzberg, G. *Molecular Spectra and Molecular Structure III. Electronic Spectra and Electronic Structure of Polyatomic Molecules*; Van Nostrand Reinhold Co.: New York, NY, 1966.
(34) Birss, F. W.; Ramsay, D. A.; Till, S. M. Further High Resolution Studies of the System of Formaldehyde. *Can. J. Phys.* **1978**, *56*, 781−785.
(35) Clouthier, D. J.; Ramsay, D. A. The Spectroscopy of Formaldehyde and Thioformaldehyde. *Annu. Rev. Phys. Chem.* **1983**, *34*, 31−58.
(36) Feng, L.; Demyanenko, A. V.; Reisler, H. O-D Bond Dissociation from the 3s State of Deuterated Hydroxymethyl Radical (CH_2OD). *J. Chem. Phys.* **2003**, *118*, 9623−9628.
(37) Feng, L.; Huang, X.; Reisler, H. Photodissociative Spectroscopy of the Hydroxymethyl Radical (CH_2OH) in the 3s and $3p_x$ States. *J. Chem. Phys.* **2002**, *117*, 4820−4824.
(38) Feng, L.; Reisler, H. Photodissociation of the Hydroxymethyl Radical from the $2^2A''(3p_z)$ State: H_2CO and HCOH Products. *J. Phys. Chem. A* **2004**, *108*, 9847−9852.
(39) Ryazanov, M.; Rodrigo, C.; Reisler, H. Overtone-induced Dissociation and Isomerization Dynamics of the Hydroxymethyl Radical (CH_2OH and CD_2OH). II. Velocity Map Imaging Studies. *J. Chem. Phys.* **2012**, *136*, 084305.
(40) Hoffman, B. C.; Yarkony, D. R. Photodissociation of the Hydroxymethyl radical. I. The Role of Conical Intersections in Line Broadening and Decomposition Pathways. *J. Chem. Phys.* **2002**, *116*, 8300−8306.
(41) Yarkony, D. R. Statistical and Nonstatistical Nonadiabatic Photodissociation from the First Excited State of the Hydroxymethyl Radical. *J. Chem. Phys.* **2005**, *122*, 084316.
(42) Townsend, D.; Minitti, M. P.; Suits, A. G. Direct Current Slice Imaging. *Rev. Sci. Instrum.* **2003**, *74*, 2530−2539.
(43) Townsend, D.; Lahankar, S. A.; Lee, S. K.; Chambreau, S. D.; Suits, A. G.; Zhang, X.; Rheinecker, J.; Harding, L. B.; Bowman, J. M. The Roaming Atom: Straying from the Reaction Path in Formaldehyde Decomposition. *Science* **2004**, *306*, 1158−1161.
(44) Gebhardt, C. R.; Rakitzis, T. P.; Samartzis, P. C.; Ladopoulos, V.; Kitsopoulos, T. N. Slice Imaging: A New Approach to Ion Imaging and Velocity Mapping. *Rev. Sci. Instrum.* **2001**, *72*, 3848−3853.
(45) Ryazanov, M. Development and Implementation of Methods for Sliced Velocity Map Imaging. Studies of Overtone-induced Dissociation and Isomerization Dynamics of Hydroxymethyl Radical (CH_2OH and CD_2OH). *Dissertation*, University of Southern California, Los Angeles, 2012.
(46) Li, W.; Chambreau, S. D.; Lahankar, S. A.; Suits, A. G. Megapixel Ion Imaging with Standard Video. *Rev. Sci. Instrum.* **2005**, *76*, 063106.
(47) Toomes, R. L.; Samartzis, P. C.; Rakitzis, T. P.; Kitsopoulos, T. N. Slice Imaging of H-atom Photofragments: Effects of the REMPI Detection Process on the Observed Velocity Distribution. *Chem. Phys.* **2004**, *301*, 209−212.
(48) Ryazanov, M.; Reisler, H. Improved Sliced Velocity Map Imaging Apparatus Optimized for H Photofragments. *J. Chem. Phys.* **2013**, *138*, 144201.
(49) *SIMION* 8.0; Scientific Instrument Services, Inc.: Ringoes, NJ.
(50) Johnson, R. D., III; Hudgens, J. W. Structure and Thermochemical Properties of Hydroxymethyl (CH_2OH) Radicals and Cations Derived from Observations of $\tilde{B}\,^2A'(3p) \leftarrow \tilde{X}\,^2A''$ Electronic Spectra and from *ab initio* Calculations. *J. Phys. Chem.* **1996**, *100*, 19874−19890.
(51) Terentis, A. C.; Kable, S. H. Near Threshold Dynamics and Dissociation Energy of the Reaction $H_2CO \rightarrow$ HCO+ H. *Chem. Phys. Lett.* **1996**, *258*, 626−632.
(52) Zhang, X. B.; Rheinecker, J. L.; Bowman, J. M. Quasiclassical Trajectory Study of Formaldehyde Unimolecular Dissociation: $H_2CO \rightarrow H_2$ + CO, H + HCO. *J. Chem. Phys.* **2005**, *122*, 14313.
(53) van Zee, R. D.; Foltz, M. F.; Moore, C. B. Evidence for a Second Molecular Channel in the Fragmentation of Formaldehyde. *J. Chem. Phys.* **1993**, *99*, 1664−1673.
(54) Reid, D. L.; Hernández-Trujillo, J.; Warkentin, J. A Theoretical Study of Hydroxycarbene as a Model for the Homolysis of Oxy- and Dioxycarbenes. *J. Phys. Chem. A* **2000**, *104*, 3398−3405.
(55) Shepler, B. C.; Epifanovsky, E.; Zhang, P.; Bowman, J. M.; Krylov, A. I.; Morokuma, K. Photodissociation Dynamics of Formaldehyde Initiated at the T_1/S_0 Minimum Energy Crossing Configurations. *J. Phys. Chem. A* **2008**, *112*, 13267−13270.
(56) Aristov, V.; Conroy, D.; Reisler, H. Symmetry and Lifetime of the Hydroxymethyl Radical in the 3p Rydberg State. *Chem. Phys. Lett.* **2000**, *318*, 393−401.